7th Power Electronics, Drive Systems & Technologies Conference (PEDSTC 2016)
16-18 Feb. 2016, Iran University of Science and Technology, Tehran, Iran

An Adaptive Recursive Discrete Fourier Transform Technique for the Reference Current Generation of Single-Phase Shunt Active Power Filters

Mohammad-Sadegh Karbasforooshan, *Student Member, IEEE,* and Mohammad Monfared, *Senior Member, IEEE*
Department of Electrical Engineering, Faculty of Engineering
Ferdowsi University of Mashhad
Mashhad, Iran
m.karbasforooshan.1991@ieee.org, m.monfared@um.ac.ir

***Abstract*—This paper proposes a novel adaptive recursive discrete Fourier transform (ARDFT) technique for the reference current generation of single-phase shunt active power filters (APFs). The suggested method is robust to input frequency changes and exactly extracts the reference current of the APF. Modeling of the converter system and design procedure of the control parameters are presented in this paper. To confirm the theoretical results, simulation results are provided. These results show effectiveness and excellent performance of the suggested technique.**

Keywords—Active power filter (APF); discrete Fourier transform (DFT); recursive Fourier transform; phase locked loop (PLL).

I. INTRODUCTION

Nowadays, the utilization of nonlinear loads, such as CFLs, LEDs, computers, electronic drives and so on is more increased in the grid. These loads cause power quality problems, additional losses, stability problems and create resonance, fault in the protection systems, electromagnetic interference (EMI), damage to the power system equipment and etc. To solve these problems, many type of compensators are introduced. Passive filters are the first compensators that introduced for the current harmonics elimination and the power factor improvement. Although passive filters have advantages of simplicity and low cost, but due to their drastic limitations, always have been used with cautions. Active power filters (APFs) are proposed to be used in distribution systems, which have the capability of eliminating the whole undesired harmonics and improving the power factor by compensating the reactive power, simultaneously [1]-[4].

Reference current generation is the most important part of the control system of APFs. Up to now, many different methods for the reference current generation of APFs are proposed in literature. These methods can be categorized into time-domain and frequency-domain techniques [5]-[7]. Fourier transform method is the most known reference current generation technique in the frequency-domain. This method provides high accuracy in harmonic detection and is used in single-phase and three-phase systems. Despite of many advantages of Fourier transform technique, this method suffers from high computational burden and high sensitivity to frequency changes of the measured signal [8]-[17].

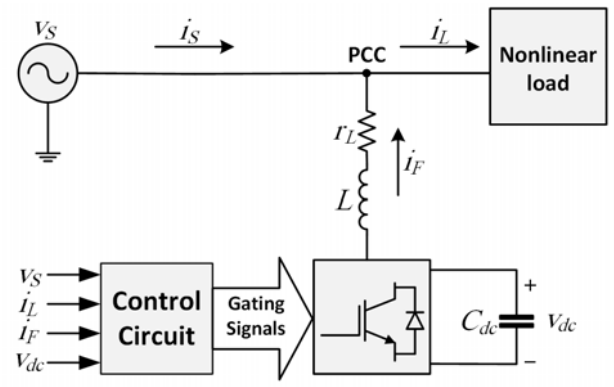

Fig. 1. Single-phase shunt active power filter.

This paper proposes a new frequency adaptive recursive discrete Fourier transform (ARDFT) structure to overcome the problems of sensitivity to input frequency changes. The paper is organized as follows: in section II, the modeling of a single-phase shunt APF and its controller parameters design are described. In section III, the proposed technique for the APF is explained. Section IV is devoted to simulation of the system with the proposed reference current generation technique. Finally, conclusion is coming in section V.

II. MODELING OF THE SINGLE-PHASE SHUNT APF AND CONTROLLERS DESIGN

A. System Modeling

Fig. 1 shows the power and control system of a single-phase shunt APF. According to this, the APF is intended to inject a compensating current, so that the grid current will be an in-phase sinusoidal waveform with grid voltage in point of common coupling (PCC). The power circuit of APF is composed of a single-phase full-bridge inverter, a DC-link capacitor and an inductor. The grid voltage includes harmonic contents and the nonlinear load is a single-phase diode rectifier that in DC-side sees a resistor parallel with a capacitor.

TABLE I. SYSTEM PARAMETERS

Parameter	*Symbol*	*Value*
DC-link voltage	V_{dc}	380 V
Grid voltage	V_S	220 V_{rms}
Inverter rating	S	2 kVA
Filter inductance	L	1 mH
ESR of the inductance	r_L	0.25 Ω
DC-link capacitance	C_{dc}	2200 uF
Grid frequency	f	50 Hz
Switching/sampling frequency	f_{sw}/f_{samp}	12.8 kHz

Table I listed system parameters. The following equation shows the inductor voltage:

$$v_F = r_L i_F + L\frac{di_F}{dt} + v_S \tag{1}$$

where L and r_L are inductance and resistance of the inductor. Equation (1) can be rewritten as

$$\frac{di_F}{dt} = \frac{1}{L}\left(v_F - r_L i_F - v_S\right) \tag{2}$$

By applying Laplace operator to (2), the transfer function of the filter current, $i_F(s)$ based on $v_F(s)$ and $v_S(s)$ is obtained as

$$I_F(s) = \frac{1}{Ls + r_L}\left(V_F(s) - V_S(s)\right) \tag{3}$$

Also, according to Fig. 1, the filter capacitor current based on average model method is [1]

$$C_{dc}\frac{d\hat{v}_{dc}}{dt} + \frac{\hat{v}_{dc}}{r_{dc}} = d\hat{i}_F \tag{4}$$

where r_{dc} represent the inverter losses. Also, the transfer function of $i_F(s)$ based on $d(s)$ assuming $v_S=0$ can be readily obtained as

$$\left.\frac{\hat{i}_F(s)}{\hat{d}(s)}\right|_{\hat{v}_S(s)\equiv 0} = \frac{2V_{dc}}{Ls} \tag{5}$$

The transfer function of $i_S(s)$ to $v_{dc}(s)$ is

$$\frac{\hat{v}_{dc}(s)}{\hat{i}_S(s)} = \frac{V_S}{2C_{dc}V_{dc}} \cdot \frac{1}{s + \left(\frac{2}{r_{dc}C_{dc}}\right)} \tag{6}$$

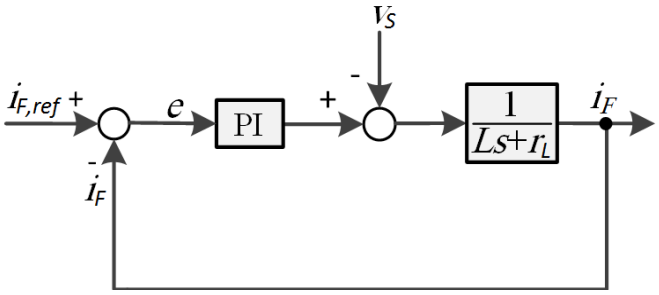

Fig. 2. Inner filter current control loop.

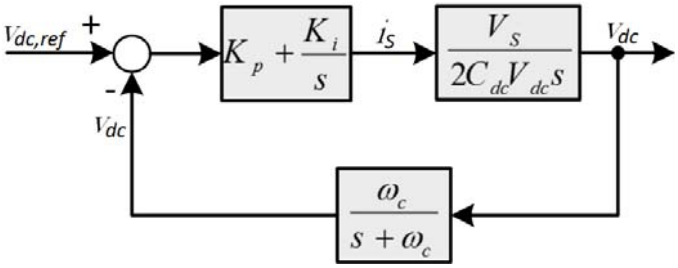

Fig. 3. Outer DC-link voltage control loop.

Therefore, by assuming that the power losses is equal to zero (r_{dc} tends to infinity), (6) simplifies to

$$\frac{\hat{v}_{dc}(s)}{\hat{i}_S(s)} = \frac{V_S}{2C_{dc}V_{dc}s} \tag{7}$$

B. Controller Parameter Design

The filter current controller is a simple proportional regulator. The inner filter current loop is shown in Fig. 2. Therefore, the closed loop transfer function of the inner loop is obtained as

$$G_I(s) = \frac{i_F(s)}{i_{F,ref}(s)} = \frac{P}{Ls + \left(r_L + P\right)} \tag{8}$$

By considering -3dB attenuation of (8) at the current bandwidth frequency, one has

$$\frac{P^2}{\left(r_L + P\right)^2 + \left(L\omega_{bi}\right)^2} = \frac{1}{2} \tag{9}$$

So, the current loop proportional gain, P is obtained as

$$P = r_L + \sqrt{2r_L^2 + L^2\omega_{bi}^2} \tag{10}$$

In this case, the current control bandwidth is considered 1000 Hz which is in the range of ten times the grid frequency (500 Hz) and one-tenth the switching frequency (1280 Hz).

To control the DC-link voltage of APF, we consider a proportional-integral (PI) controller. Also, a low-pass filter for the disturbance and noise rejection of the DC-link voltage is used. Fig. 3 shows the outer voltage control loop of APF. The closed-loop transfer function of the outer loop is

$$G_{Vdc}(s)=\frac{v_{dc}(s)}{v_{dc,ref}(s)}=\frac{V_S\left(K_p s+K_i\right)}{2C_{dc}V_{dc}s^3+2C_{dc}V_{dc}\omega_c s^2+K_pV_S\omega_c s+K_iV_S\omega_c} \quad (11)$$

Tuning the PI controller is a compromise between accessible control bandwidth and the loop stability [18]. The effect of the integral part of PI controller around the crossover and bandwidth frequency can be neglected. So, equation (11) without K_i simplified to

$$\left.\frac{v_{dc}(s)}{v_{dc,ref}(s)}\right|_{K_i\equiv 0}=\frac{V_S K_p}{2C_{dc}V_{dc}s^2+2C_{dc}V_{dc}\omega_c s+K_pV_S\omega_c} \quad (12)$$

By considering -3dB attenuation of (12) at the voltage bandwidth frequency, the proportional gain of the DC-link voltage is calculated as

$$K_p=\frac{2C_{dc}V_{dc}\omega_{bv}\left(\omega_{bv}+\omega_c\right)}{V_S\omega_c} \quad (13)$$

The voltage bandwidth frequency is always selected bellow one-tenth the grid frequency. Therefore, the voltage bandwidth is selected as ω_{bv} = 15 rad/s. On the other hand, characteristic equation of the system from (11) is

$$2C_{dc}V_{dc}s^3+2C_{dc}V_{dc}\omega_c s^2+K_pV_S\omega_c s+K_iV_S\omega_c=0 \quad (14)$$

By applying Routh-Hurwitz stability criterion to (14), the following condition is obtained.

$$K_i<K_p\omega_c \quad (15)$$

So, according to (15), the integral part of DC-link voltage controller is selected in the range [0, $K_p\omega_c$].

III. Adaptive Recursive Discrete Fourier Transform Technique

Fourier transform is one of the amplitude and phase detection methods of harmonics. The Fourier series integral in time-domain is [8]:

$$<x>_h(t)=\frac{1}{T}\int_{t-T}^{t}x(\tau)e^{jh\omega\tau}d\tau \quad (16)$$

The above equation determines harmonic coefficients of the Fourier series of the signal. The discrete form of (16) can be written as

$$<x>_h[n]=\frac{1}{N}\sum_{k=n-N+1}^{n}x[k]e^{j\frac{2\pi hk}{N}} \quad (17)$$

Equation (17) is the direct or non-recursive calculation way of discrete-time Fourier transform. This equation implies that for the calculation of amplitude and phase, a whole AC cycle information is required. Equation (17) can be rewritten as

$$<x>_h[n]=\frac{1}{N}\sum_{k=n-N+1}^{n}x[k]\left(\cos\left(\frac{2\pi hk}{N}\right)+j\sin\left(\frac{2\pi hk}{N}\right)\right) \quad (18)$$

Because of high calculation requirement of direct method, the recursive technique is already proposed. The following subsections, focus on conventional recursive method and proposed adaptive recursive method.

A. Conventional Recursive Discrete Fourier Transform

To extract the fundamental component of a signal, the recursive discrete Fourier transform (RDFT) is proposed as follows

$$\begin{cases}C_j=C_{j-1}+\frac{1}{N}\cos\left(\frac{2\pi j}{N}\right)\left(x_j-x_{j-N}\right)\\ S_j=S_{j-1}+\frac{1}{N}\sin\left(\frac{2\pi j}{N}\right)\left(x_j-x_{j-N}\right)\end{cases} \quad (19)$$

where N is the number of samples per one cycle, and S_j and C_j are the real and imaginary part of the Fourier transform. Fig. 4 shows the corresponding block diagram of equation (19). The main advantage of recursive method over the direct method is the high memory and calculation space saving. But the main limitation of the conventional recursive method is the high sensitivity to frequency changes of the input signal. Such that, the truncation, accumulation and rounding errors lead to instability of the output signal in presence of a small frequency deviation of the input signal. To clarify the situation, assume that the input signal of the Fourier transform is a pure sinusoidal waveform with 10V amplitude and 50Hz frequency. Suddenly, the frequency changed to 49.5Hz (shown in Fig. 5). The output amplitude and phase of the Fourier transform is shown in Fig. 6. As can be seen, the amplitude and phase of the output signal is unstable following the frequency change.

Therefore, the recursive method, despite the fewer memory occupation, has the major problem of instability in case of frequency changes.

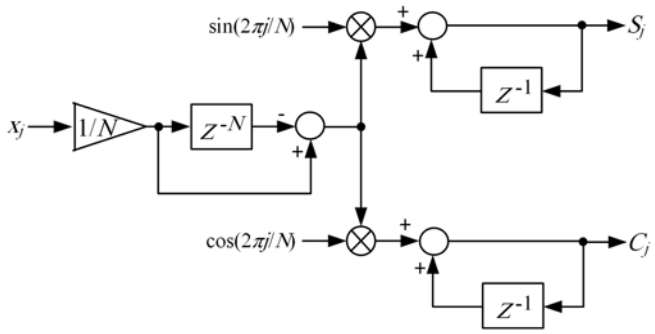

Fig. 4. Conventional recursive discrete Fourier transform.

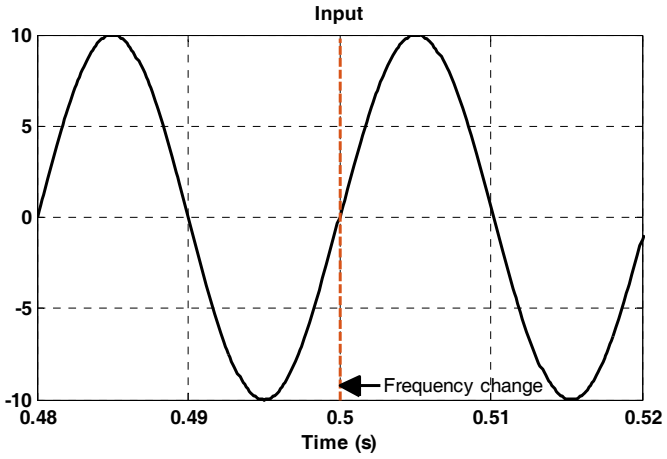

Fig. 5. A pure sinusoidal waveform with 50Hz frequency, frequency changes to 49.5Hz at t=0.5 s.

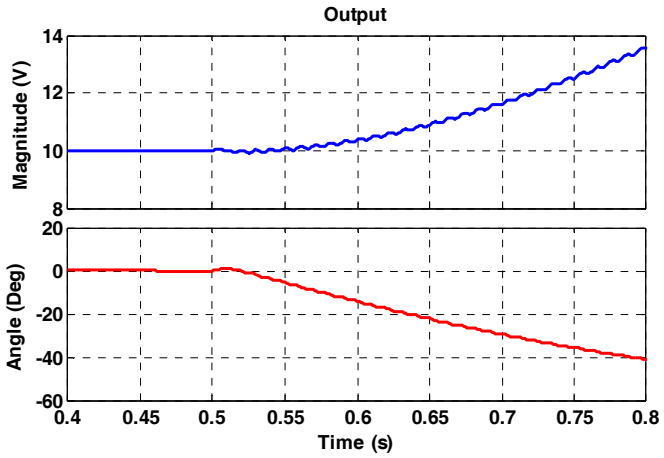

Fig. 6. Output amplitude and phase of the conventional recursive discrete Fourier transform for frequency change from 50Hz to 49.5Hz at t=0.5 s.

B. *Improved Recursive Discrete Fourier Transform*

The following equations show the improved recursive discrete Fourier transform method

$$\begin{cases} C_j = C_{j-1} + \left(P_j - P_{j-N}\right) \\ S_j = S_{j-1} + \left(M_j - M_{j-N}\right) \end{cases} \tag{20}$$

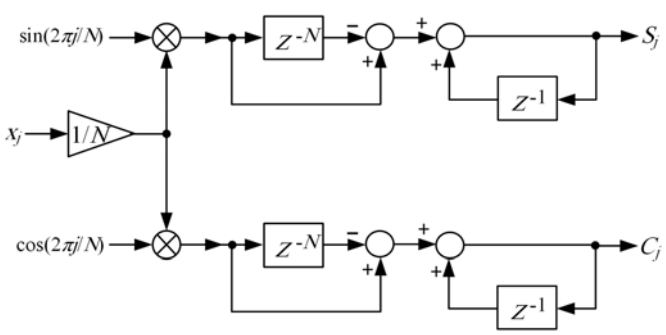

Fig. 7. Improved recursive discrete Fourier transform.

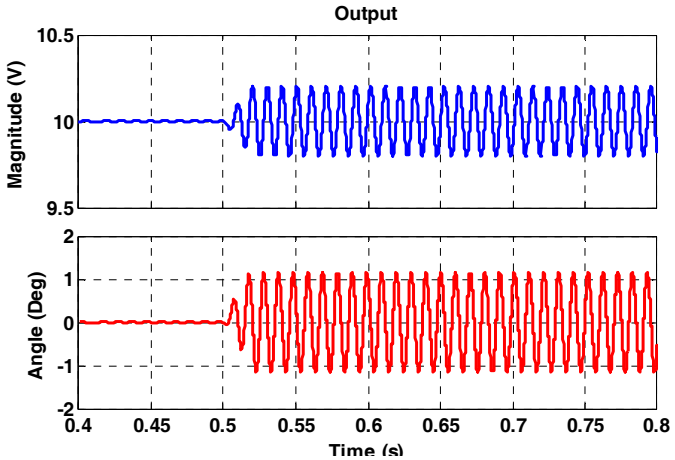

Fig. 8. Output amplitude and phase of the improved recursive discrete Fourier transform for frequency change from 50Hz to 49.5Hz at t=0.5 s.

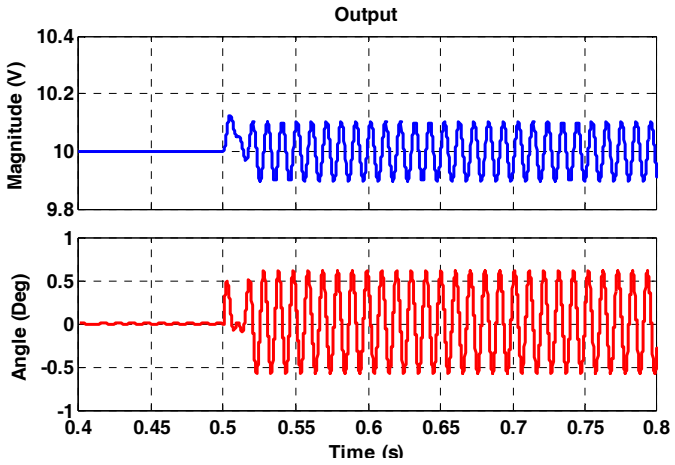

Fig. 9. Output amplitude and phase of the improved recursive discrete Fourier transform with updating *N* for frequency change from 50Hz to 49.5Hz at t=0.5 s.

where P_j and M_j are equal to $(1/N)x_j \cos(2\pi j/N)$ and $(1/N)x_j \sin(2\pi j/N)$, respectively. Fig. 7 shows the corresponding block diagram of this technique. Except adding two P_j and M_j calculations, the improved technique has no calculations more than the conventional method. In order to present the performance of this technique, the same sinusoidal waveform of Fig. 6 is applied to the improved technique and the output amplitude and phase are reported in Fig. 8. As shown in this figure, the output signal of the improved

technique remains

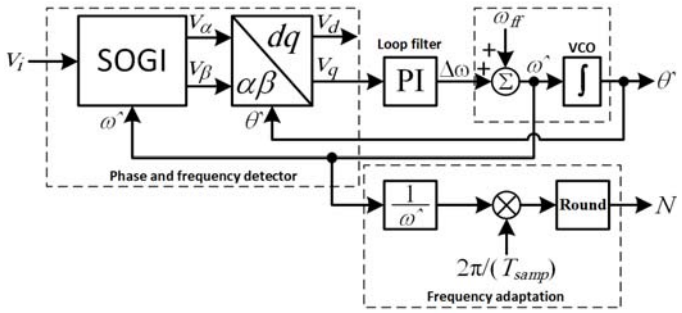

Fig. 10. Phase locked loop.

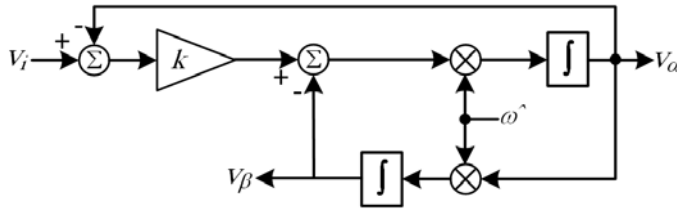

Fig. 11. Second order generalized integrator.

stable after the frequency change and only oscillates in a narrow band. These oscillations originates from the variations N as a result of the frequency change of the input signal. In the proposed technique, N is estimated continually by a phase locked loop (PLL) and its real value is used in the Fourier transform. The output result of applying sinusoidal waveform of Fig. 6 to the input of the ARDFT is shown in Fig. 9. In fact, for 10kHz sampling frequency and 50Hz fundamental frequency, the value of N was equal to 200 which by changing the frequency, the actual value of N is 202.02. By comparing Fig. 8 and Fig. 9, it can be seen that oscillations around the steady-state value have decreased. The remained oscillations are caused by the rounding error of N for the new frequency.

C. Phase Locked Loop and Frequency Adaptation

In this paper, for the calculation of the grid frequency and update of N, a second order generalized integrator (SOGI) based PLL is used that has many advantages, such as simple implementation, low computational burden, high accuracy, high speed and robust performance to disturbances. In fact, with having a PLL, two goals of grid phase and frequency extraction are fulfilled. Fig. 10 shows the PLL block diagram to extract the grid phase and frequency [5]. In this figure, v_i, θ, ω and ω_{ff} are the grid voltage, extracted phase, extracted frequency and nominal grid frequency, respectively. To calculate α and β component of the grid voltage, the SOGI block is used, which its structure is shown in Fig. 11. The SOGI provides the necessary signals for the PLL, and at the same time, creates a pure sinusoidal voltage for the reference current generation by attenuating the grid voltage harmonics and noises. The PLL provides required frequency for appropriate performance of the ARDFT technique and has an important role in increasing the system robustness against grid frequency changes.

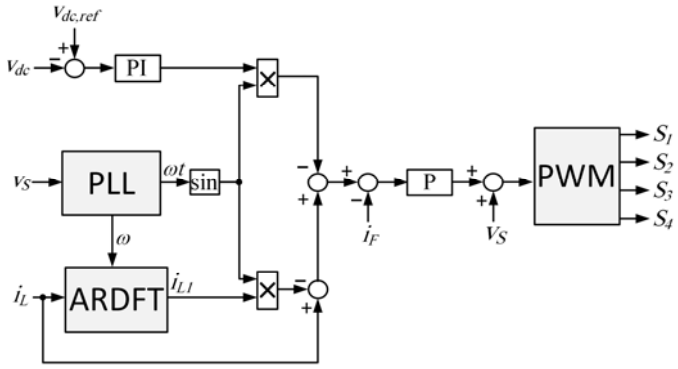

Fig. 12. Overall proposed control block diagram of the single-phase shunt active power filter.

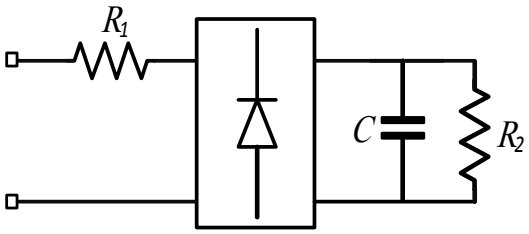

Fig. 13. Structure of the nonlinear load.

IV. Simulation Results

The overall control block diagram of the APF is shown in Fig. 12. According to Fig. 12, firstly the grid voltage phase and frequency are extracted by the PLL. Then, the ARDFT block calculates the fundamental component of the load current and by multiplying it by the voltage phase, the grid reference current is constructed. On the other hand, the difference between the DC-link voltage and its reference passes through a PI controller and by multiplying the controller output signal by the voltage phase, the filter power losses is calculated. The difference of filter current with its reference passes through a simple proportional gain. Also, in the proposed method, a feedforward path including grid voltage is added to the control signal to improve system dynamics. Finally, the resulting control signal enters PWM block and gating signals of inverter switches are produced. Table I shows the system parameters. The nominal value of N is N=12800/50=256.

In this section, different test on system in MATLAB/Simulink are done. It should be noted that the grid voltage has 5% third harmonic and 3% fifth harmonic and the nonlinear load consists of a single-phase diode rectifier as shown in Fig. 13 with R_1=1 Ω, R_2=10 Ω and C=1000 uF. The grid inductance is 20uH.

First, the steady-state response of the system is shown in Fig. 14. In this figure, the grid voltage, grid current, load current, filter current and DC-link voltage are shown. While the grid voltage THD is equal to 5.72% and load current THD is equal to 46.64%, the grid current THD is obtained equal to 2.36%. The filter current follows its reference properly and the maximum current amplitude is 25A. Also, the DC-link voltage by 2.6% ripple oscillates around the 380V reference.

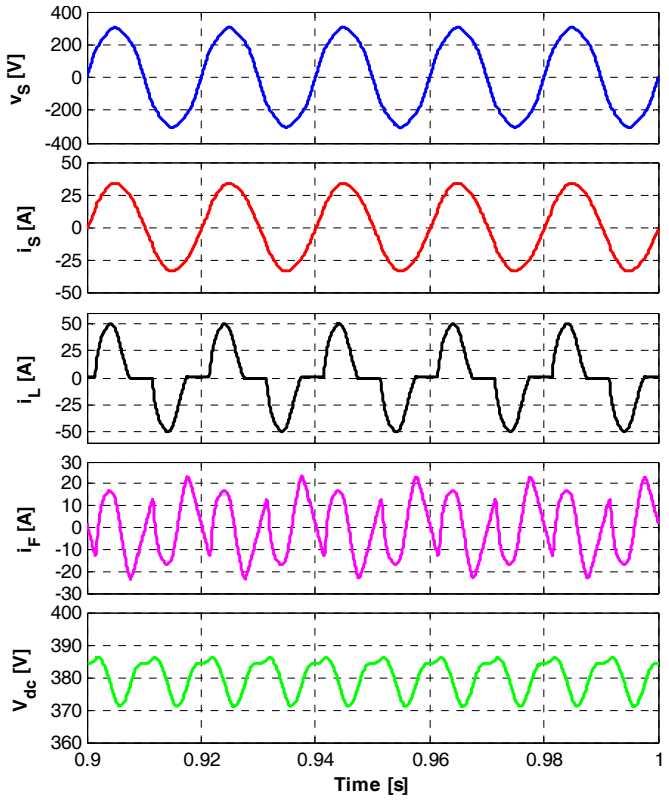

Fig. 14. Steady-state waveforms: grid voltage, grid current, load current, filter current and DC-link voltage.

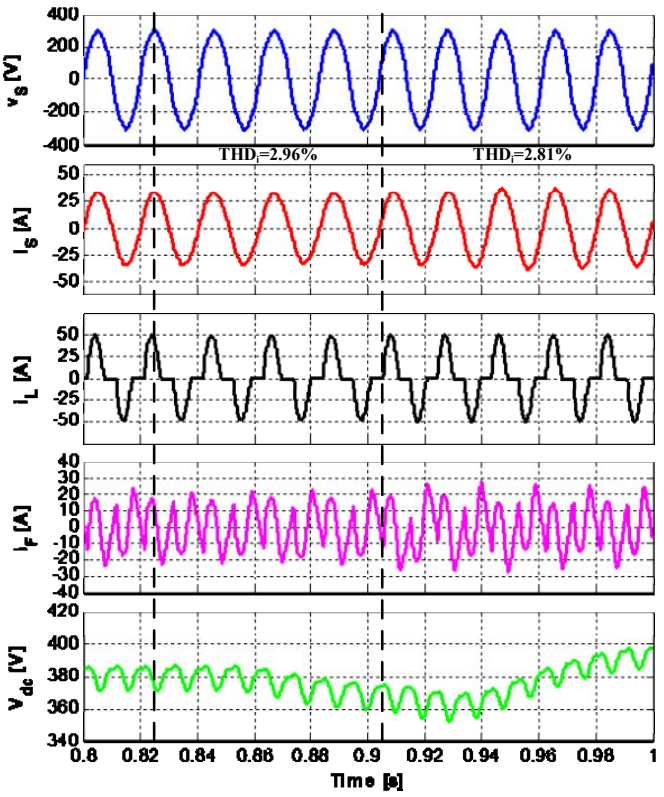

Fig. 16. Transient waveforms in response to grid voltage frequency changes: grid voltage, grid current, load current, filter current and DC-link voltage.

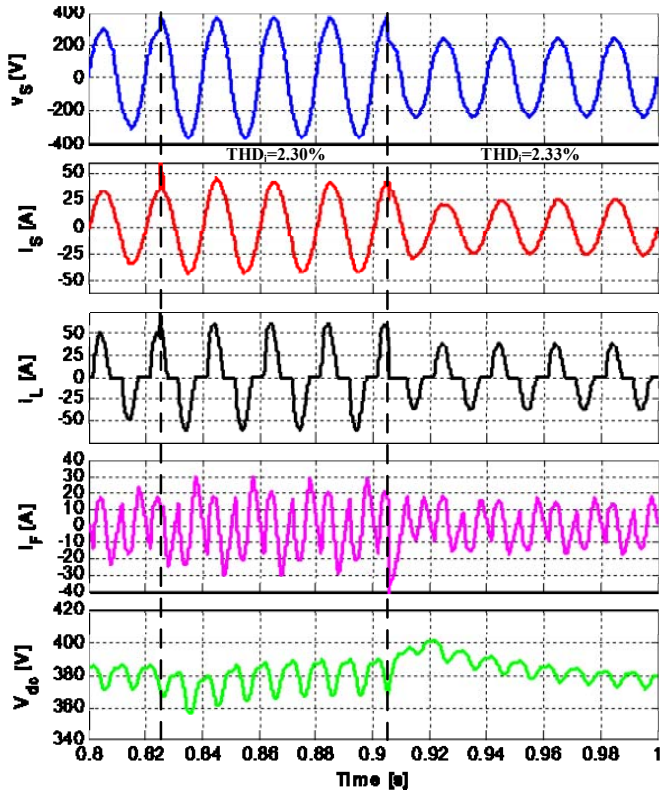

Fig. 15. Transient waveforms in response to grid voltage amplitude changes: grid voltage, grid current, load current, filter current and DC-link voltage.

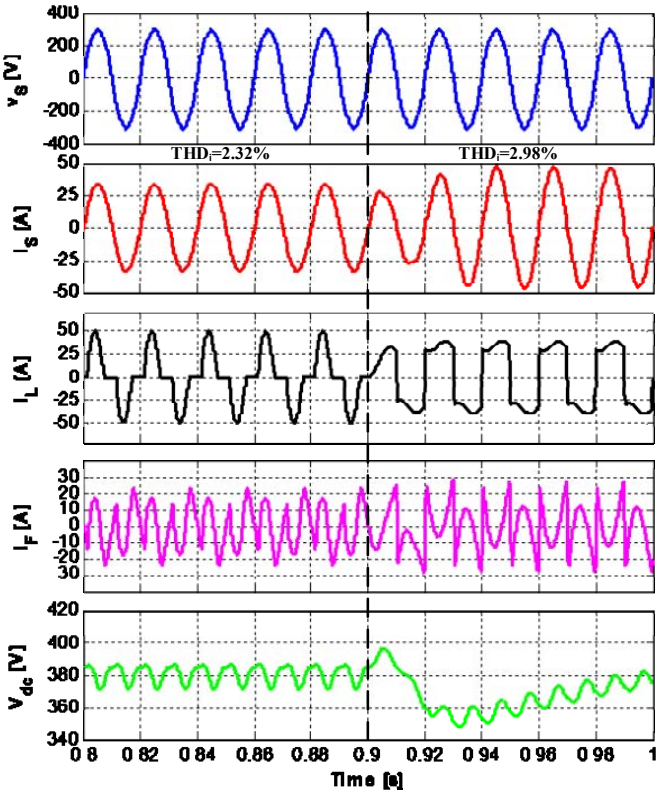

Fig. 17. Transient waveforms in response to sudden load change: grid voltage, grid current, load current, filter current and DC-link voltage.

In the next test, the transient behavior of the system against grid voltage amplitude and grid frequency changes is analyzed. Figs. 15 and 16 show the output result of these tests. In Fig. 15, the grid voltage amplitude jumped 20% at t=0.825 s and the fell 50% at t=0.905 s. In Fig. 16, the grid voltage frequency changes from 50Hz to 47.5Hz at t=0.825 s and from 47.5Hz to 52.5Hz at t=0.905 s. As can be seen in Fig. 15, a little change in the grid current and DC-link voltage occurred at the moment of sudden change of grid voltage amplitude, but the current control system acts quickly and the current attain to its steady-state in less than one cycle. According to Fig. 16, the grid frequency change has no effect on the control system and reference current generation performance, and this shows excellent and robust performance of the proposed technique. It should be noted that in two above tests, the grid current THD remains in [2% - 3%] range.

In the final test, a nonlinear load consists of a single-phase rectifier along with a 5Ω resistor series with a 30mH inductor in DC-side enters to the system at t=0.9 s and previous load is disconnected. The output result of this test is shown in Fig. 17. Despite the load change from capacitive to inductive, the grid current THD remains 3% and accurate performance of the reference current generation is well done.

V. Conclusion

This paper proposed an adaptive recursive discrete Fourier transform technique for the reference current generation of single-phase shunt APFs. The proposed technique has advantages of simplicity, high accuracy in current extraction, less calculation burden than non-recursive Fourier transform and robust performance to the frequency changes. To confirm the theoretical achievements, simulation results are presented. The results show excellent performance of the control system and the reference current generation in steady-state and transient conditions.

References

[1] S. Rahmani, K. Al-Haddad, F. Fnaiech, and P. Agarwal, "Modified PWM with indirect current control technique applied to a single-phase shunt active power filter topology," *Can. J. Electr. Comput. Eng.*, vol. 31, no. 3, pp. 135–144, 2006.

[2] F. Pottker de Souza and I. Barbi, "Single-phase active power filters for distributed power factor correction," *2000 IEEE 31st Annu. Power Electron. Spec. Conf. Conf. Proc. (Cat. No.00CH37018)*, vol. 1, no. c, pp. 500–505, 2000.

[3] S. Rahmani, K. Al-Haddad, and H. Y. Kanaan, "A comparative study of shunt hybrid and shunt active power filters for single-phase applications: Simulation and experimental validation," *Math. Comput. Simul.*, vol. 71, no. 4–6, pp. 345–359, Jun. 2006.

[4] J. Miret, M. Castilla, J. Matas, J. M. Guerrero, and J. C. Vasquez, "Selective harmonic-compensation control for single-phase active power filter with high harmonic rejection," *IEEE Trans. Ind. Electron.*, vol. 56, no. 8, pp. 3117–3127, Aug. 2009.

[5] S. Golestan, M. Monfared, and J. M. Guerrero, "Second order generalized integrator based reference current generation method for single-phase shunt active power filters under adverse grid conditions," in *4th Annual International Power Electronics, Drive Systems and Technologies Conference (PEDSTC)*, pp. 510-517, 2013.

[6] M. I. M. Montero, E. R. Cadaval, and F. B. Gonzalez, "Comparison of control strategies for shunt active power filters in three-phase four-wire systems," *IEEE Trans. Power Electron.*, vol. 22, no. 1, pp. 229–236, Jan. 2007.

[7] B. N. Singh, V. Khadkikar, and A. Chandra, "Generalised single-phase p-q theory for active power filtering: simulation and DSP-based experimental investigation," *IET Power Electron.*, vol. 2, no. 1, pp. 67–78, Jan. 2009.

[8] M. Dogruel and H. H. Çelik, "Harmonic control arrays method with a real time application to periodic position control," *IEEE Trans. Control Syst. Technol.*, vol. 19, no. 3, pp. 521–530, May 2011.

[9] K. Borisov and H. Ginn, "A computationally efficient RDFT-based reference signal generator for active compensators," *IEEE Trans. Power Deliv.*, vol. 24, no. 4, pp. 2396–2404, Oct. 2009.

[10] M. S. Reza, M. Ciobotaru, and V. G. Agelidis, "A recursive DFT based technique for accurate estimation of grid voltage frequency," in *IECON 2013 - 39th Annual Conference of the IEEE Industrial Electronics Society*, pp. 6420–6425, 2013.

[11] H. L. Ginn, "CPC based converter control for systems with non-ideal supply voltage," in *2010 International School on Nonsinusoidal Currents and Compensation*, pp. 117–122, 2010.

[12] L. Asiminoael, F. Blaabjerg, and S. Hansen, "Detection is key - harmonic detection methods for active power filter applications," *IEEE Ind. Appl. Mag.*, vol. 13, no. 4, pp. 22–33, Jul. 2007.

[13] H. L. Ginn and G. Chen, "Digital control method for grid-connected converters supplied with nonideal voltage," *IEEE Trans. Ind. Informatics*, vol. 10, no. 1, pp. 127–136, Feb. 2014..

[14] S. A. Gonzalez, R. Garcia-Retegui, and M. Benedetti, "Harmonic computation technique suitable for active power filters," *IEEE Trans. Ind. Electron.*, vol. 54, no. 5, pp. 2791–2796, Oct. 2007.

[15] S. Lai, S. Lei, C. Chang, C. Lin, and C. Luo, "Low computational complexity, low power, and low area design for the implementation of recursive DFT and IDFT algorithms," *IEEE Trans. Circuits Syst. II Express Briefs*, vol. 56, no. 12, pp. 921–925, Dec. 2009.

[16] H. A. Darwish and M. Fikri, "Practical considerations for recursive DFT implementation in numerical relays," *IEEE Trans. Power Deliv.*, vol. 22, no. 1, pp. 42–49, Jan. 2007.

[17] J. M. Maza-Ortega, J. A. Rosendo-Macias, A. Gomez-Exposito, S. Ceballos-Mannozzi, and M. Barragan-Villarejo, "Reference current computation for active power filters by running DFT techniques," *IEEE Trans. Power Deliv.*, vol. 25, no. 3, pp. 1986–1995, Jul. 2010.

[18] M. Monfared, S. Golestan, and J. M. Guerrero, "Analysis, design and experimental verification of a synchronous reference frame voltage control for single-phase inverters," *IEEE Trans. Ind. Electron.,* vol. 61, no. 1, pp. 258-269, Jan. 2014.